Preparation of Oriented Multilayers of Poly(silane)s by the Langmuir–Blodgett Technique

F. W. Embs,[†] G. Wegner,*[,†] D. Neher,[†,⊥] P. Albouy,[†,∥] R. D. Miller,[‡] C. G. Willson,[‡] and W. Schrepp[§]

Max-Planck-Institut für Polymerforschung, Ackermannweg 10, D-6500 Mainz, Germany, IBM Almaden Research Center, 650 Harry Road, San Jose, California 95720, and BASF AG, D-6700 Ludwigshafen, Germany

Received October 29, 1990; Revised Manuscript Received March 28, 1991

ABSTRACT: The spreading behavior of poly(silane)s at the air–water interface of a Langmuir trough was investigated. Force–area diagrams of poly(silane)s with various side groups and different molecular weights were recorded. Stable monomolecular layers were not obtained for alkyl substituents. In the case of *p*-alkoxyphenyl and, even better, *m*-alkoxyphenyl residues attached to the silicon backbone, stable monolayers were obtained that could be transferred to solid hydrophobic substrates by applying the Langmuir–Blodgett technique. These transferable poly(silane)s have a rodlike shape and form dense rafts at the water surface. Multilayers consisting of up to 600 monolayers of this raftlike structure with the rods preferentially oriented into the dipping direction have been obtained. The order parameter describing the degree of orientation of the rods with regard to the dipping direction was determined from the dichroic ratio of the band of the silicon–silicon chromophores at 397 nm for the *m*-alkoxyphenyl-substituted poly(silane). The order parameter could be improved substantially by annealing the samples subsequent to deposition of the layers at temperatures up to 150 °C. Samples thus obtained have the character of a monodomain nematic liquid crystal of molecularly defined thickness. Details of the structure were further elucidated by X-ray reflection and polarized IR spectroscopy.

Introduction

Soluble high molecular mass poly(silane)s are interesting radiation-sensitive materials for which a number of applications have been described.[1] The backbones of these polymers consist of silicon atoms only, each bearing two side groups.

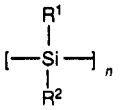

A particularly interesting feature of these materials is the delocalization of the σ-orbitals of the Si atoms in the backbone. The absorption spectra of these materials depend not only on the nature of the side groups but also on the length and the conformation of the backbone.[1-3] This spectral behavior inspired investigations of the nonlinear optical properties of poly(silane)s.[4-6] Isotropic films of poly(methylphenylsilane) are reported to have $X^{(3)}$ values between 1.5×10^{-12} esu[4] and 7.2×10^{-12} esu.[5] Higher values, up to 11×10^{-12} esu were observed in poly(di-*n*-hexylsilane).[6]

The **Langmuir–Blodgett (LB) technique** is an excellent method for the preparation of ultrathin films with a controlled thickness and a well-defined molecular order. LB films are attracting attention due to their potential applications in optical or microelectronic devices.[7] In addition to low molecular mass amphiphiles, preformed polymers have been shown to provide stable films.[8] Among the polymers, a new class of layer-forming materials has been described, namely rodlike polymers where the rods are modified by attachment of side groups with conformational flexibility and minimal polarity. Examples of such LB-forming polymers are certain substituted poly(glutamate)s in their helical conformation[9,10] and poly(phthalocyanatosiloxane)s.[11] These materials are surrounded by covalently linked conformationally mobile side groups that prevent crystallization and provide for fluidity of the monolayers.

The goal of this work was to combine the interesting properties of poly(silane)s with the advantages of the LB technique. Light-scattering measurements[12,13] and model calculations indicated that substituted poly(diphenylsilane)s have rather stiff backbones, with some analogues existing in a nearly all-trans-planar zigzag conformation that minimizes the steric hindrance of the side groups. Therefore, such molecules seemed to warrant examination in the LB technique.

This paper describes the molecular structure prerequisites and preparation conditions necessary to form Langmuir–Blodgett monolayers and multilayers from poly(silane)s together with the characterization of the structure, perfection, and properties of the multilayers obtained.

Experimental Section

Synthesis. The poly(silane)s investigated in this work were synthesized by a Wurtz-type coupling reaction starting from the corresponding disubstituted dichlorosilanes as described elsewhere.[1,14]

Film Preparation. Surface pressure–area isotherms were recorded on a commercial Lauda FW1 film balance at a rate of compression of 50 mm/min. The water for the subphase was purified by deionization followed by reversed osmosis and subsequently passed through a Millipore filtration system. Langmuir–Blodgett multilayers of poly(silane)s were prepared by using a commercial Lauda FL-1E film lift.

To avoid photodecomposition, which occurs rapidly even under moderate illumination,[1] and decomposition by electron transfer in solvents such as THF and chloroform, the poly(silane)s were spread from *n*-hexane solutions that were stored in dark vessels and all measurements were performed with exclusion of UV light. Certain very high molecular mass samples (entries 7, 8, 16a, and

† Max-Planck-Institut für Polymerforschung.
‡ IBM Almaden Research Center.
§ BASF AG.
⊥ Present address: Center of Research on Electro-Optics and Lasers, University of Central Florida, 12424 Research Parkway, Orlando, FL 32826.
∥ Present address: Laboratoire de Physique des Solides Bâtiment 510, Université Paris Sud, F-91405 Orsay, France.

0024-9297/91/2224-5068$02.50/0

Table I
Investigated Polymers

polymer	substituent on poly(silane)	R1	R2	MW,[a] g/mol
1	di-*n*-pentyl	C_5H_{11}	C_5H_{11}	23 000
2	*n*-hexyl-*n*-butyl	C_6H_{13}	C_4H_9	37 000
3	*n*-hexyl-*n*-pentyl	C_6H_{13}	C_5H_{11}	38 000
4	di-*n*-hexyl	C_6H_{13}	C_6H_{13}	28 000
5	diisohexyl	C_6H_{13}	C_6H_{13}	33 000
6	*n*-hexylisohexyl	C_6H_{13}	C_6H_{13}	32 000
7	*n*-hexyl-*n*-heptyl	C_6H_{13}	C_7H_{15}	1.0×10^6
8	di-*n*-tetradecyl	$C_{14}H_{29}$	$C_{14}H_{29}$	1.0×10^6
9	methylphenyl	CH_3	C_6H_5	
10	bis(*m*-hexylphenyl)	C_4H_4-*m*-C_6H_{13}	C_4H_4-*m*-C_6H_{13}	
11	bis(*p*-butylphenyl)	C_4H_4-*p*-C_4H_9	C_4H_4-*p*-C_4H_9	9 000
12	(*p*-methoxyphenyl)methyl	C_4H_4-*p*-OCH_3	CH_3	67 000
13	[*p*-(octyloxy)phenyl]methyl	C_4H_4-*p*-OC_8H_{17}	CH_3	15 000
14	*p*-(butoxyphenyl)-*p*-tolyl	C_4H_4-*p*-OC_4H_9	C_4H_4-*p*-CH_3	12 500
15	*p*-(butoxyphenyl)-*p*-(butylphenyl)	C_4H_4-*p*-OC_4H_9	C_4H_4-*p*-C_4H_9	18 500
16a	bis(*p*-butoxyphenyl)	C_4H_4-*p*-OC_4H_9	C_4H_4-*p*-OC_4H_9	10 000
16b	bis(*p*-butoxyphenyl)	C_4H_4-*p*-OC_4H_9	C_4H_4-*p*-OC_4H_9	1.0×10^6
17a	bis(*m*-butoxyphenyl)	C_4H_4-*m*-OC_4H_9	C_4H_4-*m*-OC_4H_9	15 000
17b	bis(*m*-butoxyphenyl)			1.8×10^6
	copolymers	monomer 1	monomer 2	
18	diphenyl/*n*-hexylmethyl	$Si(C_4H_5)_2$	$H_3CSiC_6H_{13}$	
19	diphenyl/di-*n*-hexyl	$Si(C_4H_5)_2$	$Si(C_6H_{13})_2$	22 000
20	bis(*p*-butoxyphenyl)/dimethyl	$Si(C_4H_4$-*p*-$OC_4H_9)_2$	$Si(CH_3)_2$	

[a] Weight-average molecular mass.

17a in Table I) had to be dissolved in chloroform due to their limited solubility in *n*-hexane. The solutions were all prepared at a concentration of about 0.2 g/L.

Silicon wavers, quartz slides, and glass slides were cleaned with chloroform in an ultrasonic bath for 15 min and then treated with a hot solution of $NH_4OH:H_2O_2:H_2O$ (1:1:5) for 20 min and finally rinsed with purified water for 10 min. Hydrophobic surfaces were obtained by treating the clean and dry substrates with a hot solution of hexamethyldisilazane in chloroform (1:5) for 20 min followed by a short rinse with chloroform and drying under a stream of gaseous nitrogen. Annealing subsequent to deposition was carried out in an evacuated drying oven at temperatures between 60 and 175 °C.

Film Characterization. X-ray reflection was recorded from samples consisting of 10–38 monolayers on float glass with an X-ray reflectometer (Ni-filtered Cu Kα line) described in ref 15. The Bragg reflection from multilayers on glass substrates was recorded in the reflection geometry with a Philips PW 1820 vertical powder goniometer mounted on a conventional generator using a graphite analyzer[16] and the Cu Kα line (λ = 1.54 Å). In both cases, the reflection patterns were analyzed in terms of a theory for diffraction from LB films.[17,18]

Spectroscopy. UV spectra were recorded with a Perkin-Elmer Lambda-9 spectrometer. All measurements were made in transmission geometry using quartz as the substrate. The incident beam was polarized with a Glan–Thomson polarizer. The infrared measurements were carried out with a Nicolet 60 SX FTIR spectrometer. Spectra were recorded at a resolution of 4 cm^{-1}. Grazing incidence reflection spectra were measured on 2–20 layers on gold substrates by using a previously described reflection accessory.[19] Polarized transmission spectra were measured on samples with 20–30 layers on each side of a silicon wafer.

Nonlinear Optical Measurements. THG measurements were carried out as previously described[20] by using infrared pulses (t = 35 ps, λ = 1064 nm, E = 0.4 mJ/pulse) generated by an Nd:YAG laser. The samples were mounted on a rotation stage in an evacuated chamber. All experiments were performed with the 1064-nm fundamental. The s-polarized component of the third harmonic was measured as function of the angle of incidence and analyzed as described in ref 20.

In order to determine both the magnitude and the phase of $X^{(3)}$, Maker fringe patterns were recorded from a sample with a film on the back side of a fused silica substrate and from the same substrate after in situ removal of the film. A value of 3.11 $\times 10^{-14}$ esu was used for fused silica glass as the reference.

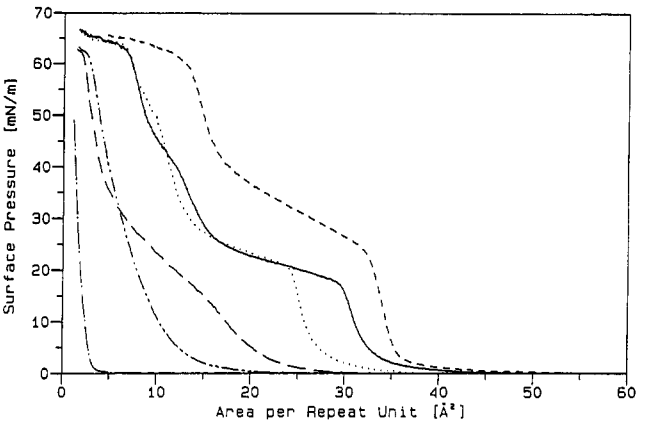

Figure 1. Surface pressure–area diagrams of poly(silane)s with different side groups at 15 °C: **4** (— · —), **10** (— ·· —), **13** (— —), **15** (···), **16** (—), **17** (– –) (13 °C) according to the entries in Table I.

Results and Discussion

Behavior at the Air–Water Interface. Surface pressure–area diagrams of six different poly(silane)s spread to the air–water interface are depicted in Figure 1. As indicated by the shape of the curves, only poly(silane)s **15–17** form monolayers that are stable at constant surface pressure. All of the other poly(silane)s exhibit behavior as exemplified by polymers **4**, **10**, and **13** in Figure 1. They do not demonstrate a well-defined step in the isotherm, which is evidence for the formation of a stable monolayer at the air–water interface. The data in Figure 1 were recorded at a subphase temperature of 15 °C, but essentially the same behavior is observed at all temperatures between 5 and 45 °C. Some characteristic values were derived from the experimental surface pressure–area curves as schematically depicted in Figure 2. The relevant data of poly(silane)s **15–17** are listed in Table II. A coherent monolayer film is formed approaching point A from the low-pressure, large-area regime. The monolayer is compressed reversibly until the region around point B is reached. Although we cannot present a detailed proof, we assume that the monolayer forms a less ordered double layer in the region between points B and C. This assumption is corroborated by the fact that the area cor-

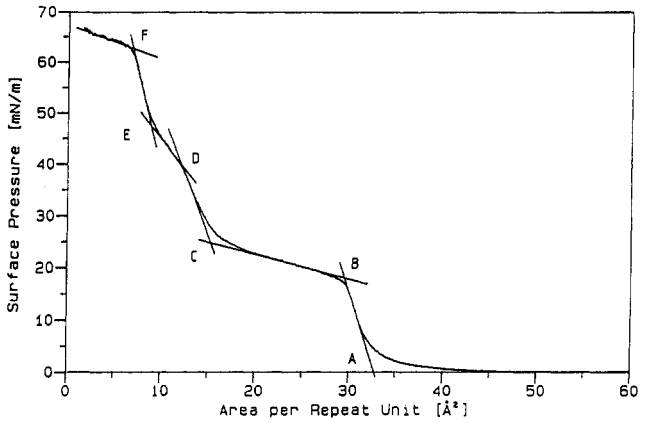

Figure 2. Characteristic points defined on an idealized surface pressure–area diagram of the type obtained from 15–17.

responding to points C and D is approximately half of the area at points A and B. Whether higher order layers are formed at points D and E and what causes the ultimate collapse at point F are not understood at present. It is worth mentioning that irreversible compression–expansion behavior is seen once the region of point B has been passed toward higher pressures and lower areas.

To further clarify the temperature dependence of the monolayer-forming ability of **15–17**, the surface pressure at points B and D is shown as a function of temperature in Figure 3. The three polymers exhibit similar behavior in the pressure–temperature region at point B but differ markedly in the behavior around point D. As will be shown later, the monolayers can be transferred to solid substrates at constant pressure in a region close to but below point B such that the rodlike molecules form a dense film with all of the rods in the plane of the substrate. The observed area per repeat unit at point B and the structure of the transferred layers are consistent with this model. There is no condition we have found under which the molecules are oriented normal to the air–water interface. In particular, there is no evidence that such a situation arises at points D and F.

The experimental values of the areas per repeat unit at point B are in good agreement with calculations based on space-filling models assuming an all-trans planar zigzag conformation of the backbone with the phenyl rings extended perpendicular to the main chain. The assumed conformation of the polymers is depicted in Figure 11 and will be discussed in more detail in conjunction with the spectroscopy data. The poly(silane)s are extremely susceptible to autoxidation and to photodegradation even by spurious exposure to daylight. This lability causes irregularities in the spreading and transfer behavior unless care is taken to exclude UV light and appropriate solvents have to be used. To demonstrate such effects, a series of surface pressure–area diagrams obtained by spreading a solution of poly(silane) **16** in THF after different periods of aging are depicted in Figure 4. The areas and pressures corresponding to points A and B are severely affected. Therefore, only freshly prepared solutions and samples stored in the dark were employed in these studies. The degradation reaction that leads to such changes in the surface area behavior is particularly enhanced by solvents that may serve as radical donators or transfer agents such as chloroform, THF, or dichloroethane.

LB Multilayers. Monolayers of **15–17** were transferred at 7 °C and at a surface pressure between 10 and 16 mN/m. The transfer ratio was equal to 1 and constant in the downstroke and the upstroke when hydrophobic substrates were covered at a dipping speed between 5 and 400 mm/min. In the case of **17**, multilayers composed of up to 600 monolayers were obtained.

X-ray Reflectometry. The structure of the LB layers transferred to solid substrates was investigated by X-ray scattering in reflection geometry. This experiment gives the overall thickness of the layer assembly and parameters describing the smoothness of the surface as well as the periodicity and quality of the layer structure. The periodicity relates to the thickness of an individual monolayer within the layer assembly.

An experimental interference pattern of the reflected intensity near the angle of total reflection is shown as the solid line in Figure 5. The simulated angular dependence of the reflectivity, represented by the dotted line, was calculated by using the following equation:[16]

$$A_1 = (r_F + r_S \exp(iqT))/(1 + r_F r_S \exp(iqT)) \quad (1)$$

where r_F is the reflectivity of the LB film, r_S the reflectivity of the substrate, q the scattering vector $4\pi \sin\theta/\lambda$ (λ = 1542 Å), and T the total film thickness. In real samples, the interfaces are always characterized by random roughness. This was taken into account by expressing the reflectivity in the form

$$r_F = \exp(-q\,\delta/2)(v - v_F)/(v + v_F) \quad (2)$$

where v and v_F are the propagation angles in air and in the sample and δ is a factor characterizing the film roughness.

Reflection from the periodic structure of the monolayer package in the LB film results in a first-order Bragg peak as shown for **17** in Figure 6. The layer spacing, d, was calculated from the reflecting angle θ by applying Bragg's law:

$$d = \lambda/(2 \sin\theta) \quad (3)$$

A theoretical correlation length l of the layer structure can be obtained from the half-width w of the Bragg peak at half-intensity by using the Debye–Scherrer formula:

$$l = 0.888\pi/w \quad (4)$$

Further, a correlation coefficient c is defined as the correlation length l divided by the total film thickness T. This coefficient varies between 0 and 1 and is a measure of the perfection of the layer structure. The values derived from the experimentally recorded reflection data were not corrected for collimation errors or other instrumental artifacts. Corrections due to these effects were considered to be small compared to the desired precision with which the data were necessary in order to support the molecular architecture of the layer assembly.

X-ray reflection from LB films composed of 20 monolayers of polymer **17** (Figure 6a) shows a sharp first-order Bragg peak with a layer spacing of 14.6 Å and a correlation coefficient of 0.4. Annealing the samples for 1 h at 125 °C subsequent to deposition decreases the layer spacing to 14.0 Å and increases the correlation coefficient to 1 (Figure 6b). This reduction of the layer spacing during annealing is observed for all samples and independent of the number of transferred monolayers. The total film thickness (280 Å) of annealed samples obtained from small-angle X-ray reflection measurements agrees quite well with the thickness obtained from multiplying the number of transferred layers (20) by the layer periodicity (14.0 Å). LB films composed of 38 monolayers reach a calculated correlation coefficient of 0.9 under the same annealing conditions; see Table III. However, in LB films of greater thickness, the half-width of the Bragg peak is influenced significantly by the collimation error. Since effects due to the collimation error were not taken into account, which

Table II
Characteristic Values Taken from the Surface Pressure–Area Isotherms of Selected Poly(silane)s

poly(silane)		characteristic points as defined by Figure 2					
		A	B	C	D	E	F
15	π, mN/m	0.0	17.5	20.5	40.0	45.0	62.0
	A, Å	28.5	26.0	14.5	11.0	8.0	6.5
16	π, mN/m	0.0	17.5	25.0	41.0	48.5	64.0
	A, Å	33.0	30.0	15.5	12.5	9.0	7.0
17	π, mN/m	0.0	20.0	39.0			62.0
	A, Å	36.0	33.0	17.0			14.0

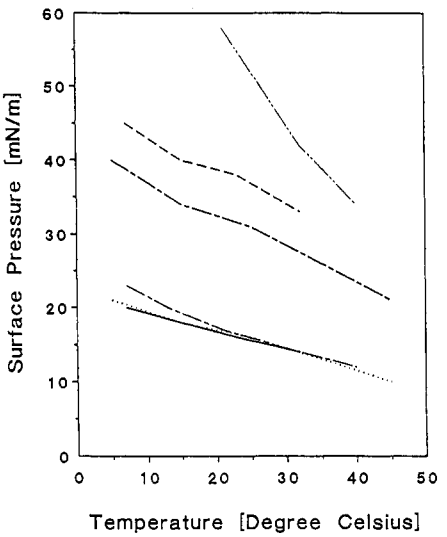

Figure 3. Monolayer stability of poly(silane)s at the air–water interface as a function of temperature. Surface pressure at point B: **15** (—), **16** (···), **17** (— –). At point D: **15** (— –), **16** (– –) **17** (— ·· —).

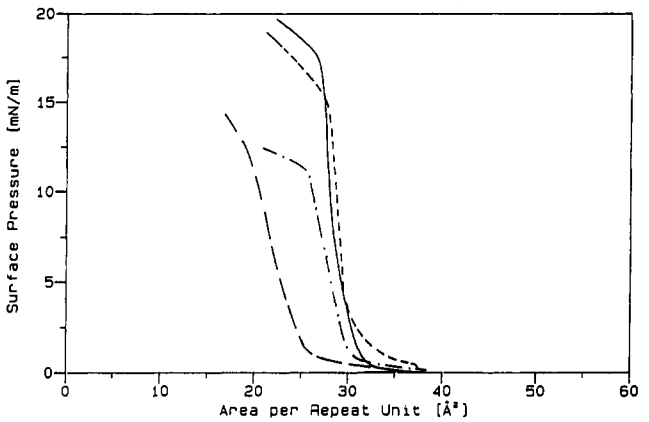

Figure 4. Decline in the stability of the monolayer of **16** when stored in THF by decomposition as a function of the time: 3 h (—), 11 days (– –), 21 days (— · —), 59 days (— —).

become significant at this total layer thickness, the decrease of c to 0.9 is worth being discussed further.

Polarized UV Spectroscopy. Polarized transmission UV spectra of LB multilayers of **15–17** on quartz substrates were measured to determine the orientation of the polymers in the plane of the LB layers. The UV spectra of the LB films show the same absorption bands as poly(silane)s in solution. The UV spectrum recorded from 40 monolayers of **17**, that is, 20 layers on each side of a quartz substrate, is depicted in Figure 8. The long-wavelength, disallowed π–π^* absorption band of the substituted phenyl ring occurs at 295 nm, and the intense and narrow band of the conjugated Si–Si backbone appears at 397 nm. Imperfections in the film and the substrate scatter light and cause a small but noticeable unstructured and continuous absorption in the visible region of the spectra.

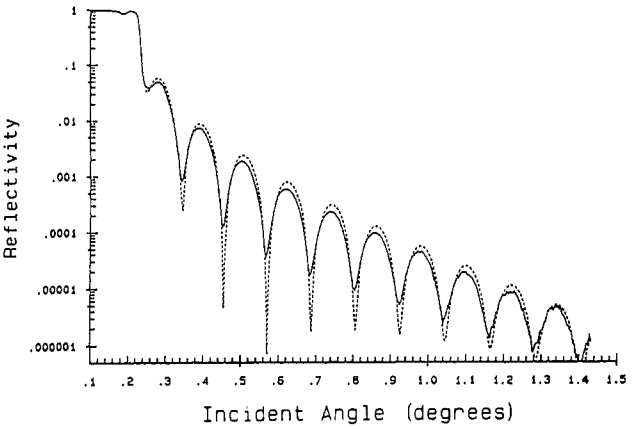

Figure 5. Small-angle X-ray reflection from 26 monolayers of **17** on float glass. Continuous line: experimental result. Dotted line: theoretical fit assuming a total layer thickness of 364 Å and a surface roughness δ = 11 Å (compare, e.g., ref 2).

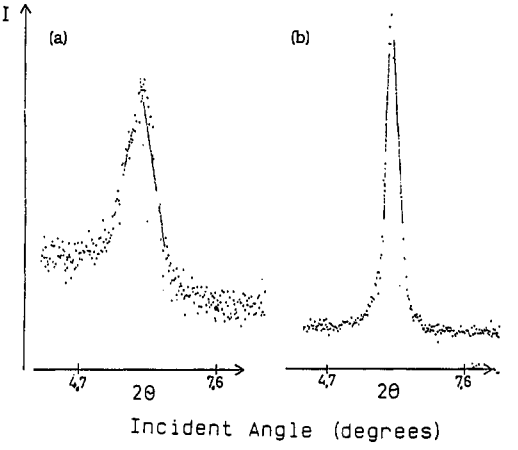

Figure 6. Bragg peak from a multilayer assembly of 20 monolayers of **17** on a quartz slide. (a) After deposition, (b) after annealing at 125 °C for 1 h.

Table III
Layer Structure and Perfection of LB Layers of Polymer 17 as a Function of the Total Number of Monolayers and Annealing Conditions

no. of layers	remarks	d, Å	l, Å	c	t, Å	δ,[a] Å
20	subsequent to	14.28	130	0.4	284	11
38	deposition	14.68	200	0.4	553	22
15	annealed	14.10	171	1.0	165	16
20	at 125 °C	13.99	281	1.0	280	11
26	for 1 h	13.98			364	11
38		13.96	470	0.9	530	16

[a] Describes a combination of the roughness arising at the interfaces air–LB layer and LB layer–substrate by a single value.

LB films of **16** are similar to that of **17**. The weak π–π^* transition occurs at 285 nm, and the conjugated backbone absorbance is shifted to 324 nm. This polymer exhibits thermochromism[14] in *tert*-butylbenzene solution as characterized by a shift of the band at 324 to 409 nm upon

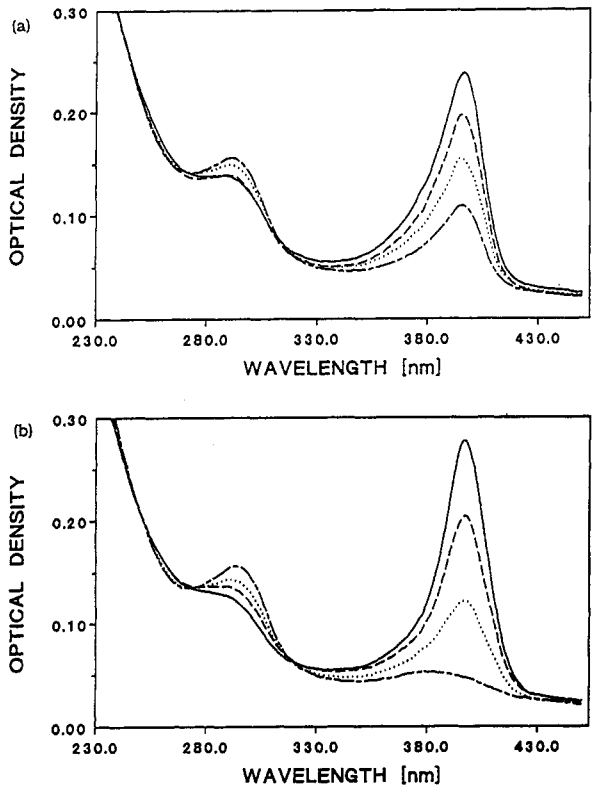

Figure 7. Transmission polarized UV spectra of 40 monolayers of 17 on quartz. Different angles between polarization and dipping direction at normal incidence are shown: (—) 0 °, (– –), 30°, (···) 60°, (— –) 90°. (a) Subsequent to deposition, (b) after annealing at 150 °C for 2 h.

heating. The onset of the thermochromic transition was seen in the LB films around 150 °C, but upon further heating, the films were destroyed and droplets of a polymeric melt were formed at 175 °C. 15 shows the phenyl absorption at 285 nm, but the polymer backbone absorbs at two wavelengths, 324 and 400 nm. The ratio of the 324-nm absorbances to that at 400 nm changes from 1.2 when measured in *n*-hexane to 0.2 in THF. The UV spectra of the corresponding LB films exhibit a ratio of 1.5 independent of the solvent from which the molecules were spread and independent of the transfer conditions. The UV spectra of the LB films of the 15–17 all exhibit strong dichroism in the plane of the substrate as depicted in Figure 7 for 17 (40 monolayers on a quartz substrate). The polymer backbone absorption at 397 nm shows the maximum extinction with the electric field vector of the polarized beam parallel to the dipping direction. The lowest absorbance occurs perpendicular to the dipping direction. The phenyl absorption at 295 nm shows exactly the opposite behavior.

The dichroic ratio R, defined as the intensity of the poly(silane) backbone absorption at its maximum (parallel to the dipping direction) divided by the intensity of the same absorption at its minimum (perpendicular to the dipping direction), is as high as 2.9 for LB multilayers of 17 when measured immediately after deposition, without any posttreatment (Figure 7a). This ratio increased to values higher than 20 when the sample was annealed for 2 h at 150 °C (Figure 7b). The orientation of the phenyl side groups was also improved markedly by annealing. Similar results are obtained from LB multilayers of 15 and 16 as listed in Table IV.

The dichroic spectra indicate a preferred orientation of the polymer backbones along the dipping direction. All of the polymers we have studied are aligned during the transfer process from the air–water interface onto the solid substrates. Polarized reflection spectra taken of the monolayers at the air–water interface during the transfer have demonstrated that the reflected intensity is independent of the angle between the polarization vector and the rim of the trough. It thus may be assumed that the alignment of the chains is a consequence of the transfer process itself. It was therefore of interest to investigate the chain length dependence of the alignment. Two samples of 17 were examined: polymer **17a**, with a mass-average contour length of 6.5 nm, and polymer **17b**, with a corresponding length of 770 nm. The dichroic ratios are approximately 2 for the high molecular mass material and 2.9 for the material of lower molecular mass. These values are independent of the number of layers deposited, as can be seen from Table IV. The exception is the very first layer in which the molecules seem to be poorly oriented, as indicated by the significantly lower value of the dichroic ratio for the first double layer. The contribution of the first layer to the relaxation behavior of the adjacent layers during annealation becomes particularly obvious upon inspecting the data of Table IV. Annealing a sample of the low molecular mass material leads to a decrease in the dichroic ratio to 1.5 for the first double layer. The ratio of the 4-layer assembly is only 5.4 compared to 11.5 for 22 monolayers under otherwise the same conditions.

Table IV
Dichroic Ratio (R) and Orientation Parameter (S) of Poly(silane)s 15, 16, 17a, and 17b in Langmuir–Blodgett Multilayers

polymer	no. of layers	untreated		annealed[a]	
		R	S	R	S
15	8	2.2[b]	0.687		
		3.2[c]	0.762		
16	10	2.9	0.743	>25[d]	>0.961
17a	20	2.9	0.743	>20[e]	>0.950
	2	2.2	0.687	1.5	0.600
17a[h]	4	2.6	0.722	5.4	0.844
	8	2.8	0.737	8.8	0.900
	14	2.9	0.743	11.5	0.920
	22	2.9	0.743	11.5	0.920
17b[i]	2	1.9	0.655	1.9	0.655
	20	1.8	0.643		
	50	2.1	0.677	3.0[f]	0.750
17b	8	1.0[g]	0.5		

[a] Annealed at 125 °C for 1 h. [b] Absorption band at 400 nm. [c] Absorption band at 324 nm. [d] Annealed at 125 °C for 4 h. [e] Annealed at 150 °C for 2 h. [f] Annealed at 140 °C for 12 h. [g] Transferred at 31 mN/m and 10 Å per repeat unit. [h] 10000 g/mol. [i] 1.8×10^6 g/mol.

These results are consistent with the model depicted in Figure 11 in which the polymer is highly oriented with transition moment of the silicon backbone aligned along the dipping direction (a) and the phenyl side groups standing perpendicular to the axis of the main chain (b). This model is further substantiated by polarized IR spectra and grazing incidence reflection measurements.

FTIR Spectroscopy. FTIR spectra were taken in grazing incidence reflection and in transmission geometry with polarized light. These spectra provide information about the orientation of individual bond vectors. Figure 8 shows three different FTIR spectra of 17 obtained from a multilayer assembly with the electric field vector in the plane of the substrate parallel to the dipping direction ($E \| D$) (a), with the vector in the plane perpendicular to the dipping direction ($E \perp D$) (b), and with the vector normal to the substrate plane (GIR) (c). The assignment of the bands is provided in Table V. These spectra show significant differences in the intensity of some vibrational bands. The phenyl out-of-plane vibration at 850 cm^{-1} is

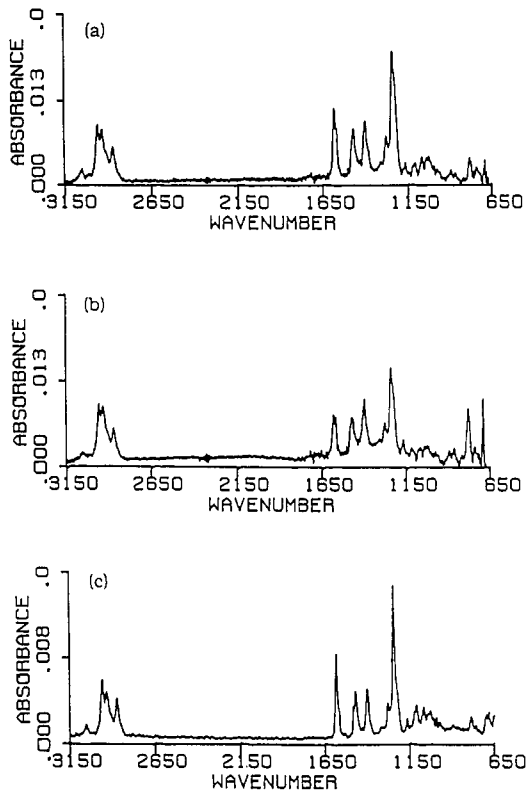

Figure 8. FTIR spectra of LB multilayers of **17**. Transmission spectra of 40 monolayers on silicon with the polarization of the electric field parallel (a) and perpendicular (b) to the dipping direction. Grazing incidence reflection (c) from 20 monolayers on a gold surface. Wavenumber in cm^{-1}.

Table V
Infrared Absorption of Polymers 16 and 17

wavenumber, cm^{-1}	assignment	$(E\|\|D)/(E\perp D)$[a] in transmission of 17	16
785 (m)	phenyl out of plane		2.00
830 (m)	phenyl out of plane	1.4	
1010 (w)	phenyl ring stretching	0.75	
1030 (w)	phenyl ring bending	1.8	
1070 (w)	CH_2O, aliph. ether	1.5	1.00
1100 (m)	Si–phenyl	0.7	0.75
1175 (s)	Si–phenyl	0.7	0.75
1245 (s)	CO, aryl–ether, sym.	0.6	0.65
1275 (s)	CO, aryl–ether, asym.	0.7	0.75
1395 (w)	CH_2O, aliph. ether, sym.	0.75	0.80
1420 (w)	phenyl stretching	0.75	0.75
1475 (m)	CH_2O, aliph. ether, asym.	0.75	0.75
1500 (s)	phenyl stretching	0.72	0.75
1565 (m)	phenyl in plane stretching	0.72	0.72
1590 (s)	phenyl in plane stretching	0.65	0.60
2872 (m)	CH_3 stretching, sym.	1.00	0.90
2933 (m)	CH_3 stretching, sym.	1.00	1.00
2959 (m)	CH_3 stretching, asym.	1.00	1.00
3010 (w)	phenyl CH stretching		0.65

[a] Absorption ratio.

more intense when the polarization is parallel to the dipping direction ($E\|\|D$), whereas the phenyl in-plane vibration at 1595 cm^{-1} shows exactly the opposite behavior. This leads to the conclusion that the planes of the phenyl rings are perpendicular to the dipping direction with the normal to their plane pointing in the parallel direction. This conclusion is supported by the fact that the out-of-plane vibration in the GIR mode is very low. The intense phenyl in-plane absorption of the GIR spectra indicates that the phenyl rings lie in a plane that is perpendicular to the substrate plane. Further, the ether vibration at 1240 cm^{-1} shows a strong dichroism with higher absorbance in the perpendicular mode ($E\perp D$) and a very intense band in the GIR spectra. This indicates that the ether bonds lie in a plane that is perpendicular to the substrate and at 90° to the dipping direction. The transition moment of the C–O bond forms an angle between 0 and 90° with the plane of the substrate. The CH region from 2800 to 3000 cm^{-1} does not exhibit any measurable dichroism. These results are summarized and translated into a molecular orientation model shown in Figure 11.

Table VI
$X^{(3)}$ Values of the Poly(silane)s 16 and 17

poly(silane)	orientation[a]	Re $[X^{(3)}]$, 10^{-12} esu		Im $[X^{(3)}]$, 10^{-12} esu	
16	$E\|\|D$	0.9	0.3	0.3	0.2
	$E\perp D$	0.5	0.3	0.1	0.2
17	$E\|\|D$	−2.7	0.3	0.5	0.5
	$E\perp D$	−1.4	0.2	0.5	0.3
17[b]	$E\|\|D$	−4.2	0.5	0.8	0.7
	$E\perp D$	−0.2	0.3	0.5	0.2

[a] Orientation of the electric field vector E to the dipping direction D. [b] Sample annealed at 120 °C for 1 h.

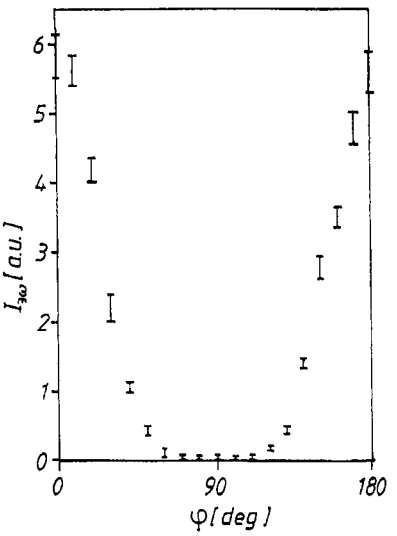

Figure 9. $X^{(3)}$ values of an LB multilayer of **17** as a function of the angle between the dipping direction and the electric field vector after annealing at 125 °C for 1 h.

Nonlinear Optical Properties. The results of the Maker fringe experiments on LB films of **16** and **17** are summarized in Table VI. All values of $X^{(3)}$ obtained are larger with the polarization of the fundamental light parallel to the dipping direction than with it perpendicular to it. This strong anisotropy of the nonlinear optical effect in the plane of the substrate is consistent with the model described above and shown in Figure 11. The angular dependence of $X^{(3)}$ is depicted in Figure 9. These results lead to the conclusion that $X^{(3)}$ at 1064 nm is strongly dominated by the oscillator strength of the poly(silane) backbone and less influenced by the phenyl absorption. The anisotropy was strongly enhanced by annealing under the conditions described above (Table VI), resulting in an maximum absolute value of 4×10^{-12} esu. The shift of the absorption maxima from 325 nm of **16** to 400 nm of **17** is accompanied by an increase in $X^{(3)}$. This can be attributed to an increase in the effective conjugation length along the polymer backbone in the latter polymer assembly.

Conclusion

The conformation of poly(silane)s is markedly influenced by the steric interactions between the side chains. Attaching two substituted phenyl rings to each silicon atom

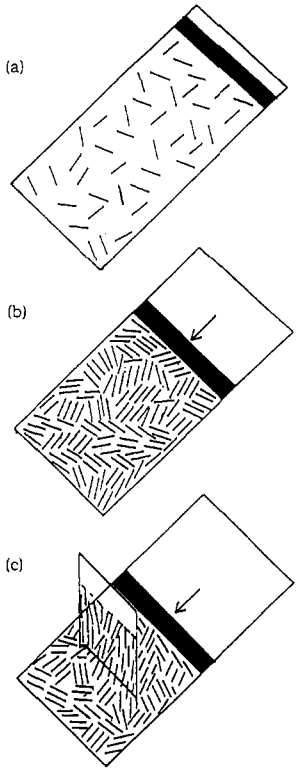

Figure 10. Schematic depiction of LB preparation of rodlike polymers. (a) Spreading of the polymers from solution. (b) Compressing to form a monolayer. (c) Transfer to a solid substrate.

as in the 15–17 leads the silicon backbone to adopt an all-trans planar zigzag conformation in which the phenyl rings are oriented approximately perpendicular to the main chain axis, as depicted in the Newman projection in Figure 11a. In this configuration, the phenyl rings, having a diameter of about 5.6 Å and a thickness of 3.6 Å, stack approximately parallel to one another and exhibit only a small rotational mobility. This conformational restriction results in significant stiffness in the main chain. Experimental confirmation of the stiffness is obtained from light-scattering measurements that show a persistence length of over 100 Å for poly[bis[*p*-(*n*-butyl)phenyl]silane].[13] Poly(silane)s having a total contour length in the order of the persistence length behave as rodlike polymers.

The alkyl and alkoxy substituents attached to the phenyl rings exhibit conformational disorder and prevent these rodlike polymers from crystallizing. Additional disorder occurs in 17, which has two possible rotameric states of the meta-substituted phenyl rings as depicted in Figure 11a. 16 exhibits less disorder around the central stiff backbone, and 15 shows only half the number of polarizable groups in the outer shell of the molecule. None of the polymers investigated bear amphiphilic groups in the main chain or in the side groups. Therefore, monolayers are not formed as result of the polarity influences mentioned in the generally accepted description of LB monolayer formation by amphiphilic molecules. As seen from Figure 1, compression of totally hydrophobic polymers give areas per repeat that are too small compared with any molecular model one could imagine (2–4 Å). In addition, defined steps in the surface pressure–area diagrams are not observed. Comparing the surface pressure–area diagrams of 4 and 10 with those of 13 and 15–17 in Figure 1, it is apparent that some small polarity in the side groups is essential for these polymers to be spread on the water surface in a way such that they are arranged side by side

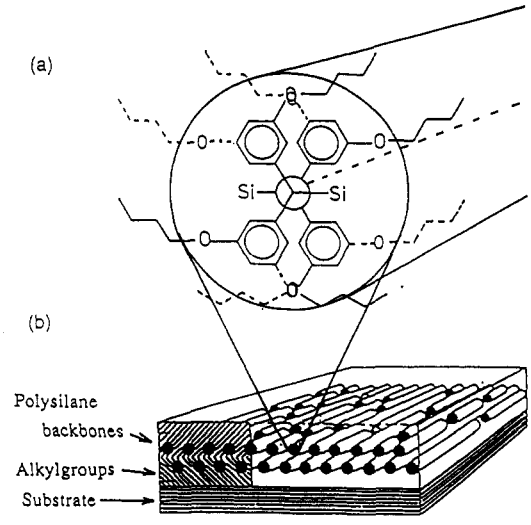

Figure 11. Molecular orientation of the transferred poly(silane)s in the LB multilayers. (a) Orientation of the side groups with regard to the main chain. (b) Alignment of the polymer backbones in the layer plane.

and not on top of one another, Figure 10a. The polymers with some polar side chain functionality distributed around the cylindrical surface of the macromolecule show a step and a surface pressure at an area per repeat unit that corresponds to values derived from model calculations.

Rodlike polymers form a two-dimensional, nematic-type order at the air–water interface when they are compressed, as shown in Figure 10b. The variation in the area per repeat unit obtained from these poly(silane)s is related to variations in the geometry of their alkyl and alkoxy side chains. These molecules have a cylindrical geometry similar to others that we have found to form LB monolayers such as the alkyl-substituted poly(glutamate)s in their helical conformation and the rodlike poly(phthalocyanatosiloxane)s when they are similarly substituted with alkoxy groups.

15–17 behave somewhat differently during the transfer to hydrophobic substrates. The maximum transfer rate (up to 400 mm/min) is obtained in the downstroke with 17 rather than 15 and 16 (25 mm/min). This effect may be a reflection of the maximal disorder of the side groups in 17, which provide for a higher mobility of the backbone and a certain fluidity of the monolayer. This effect is also observed with poly(glutamate)s; only a special ratio of long and short side chains attached to the helical backbone provides for sufficiently fluid monolayers to allow efficient transfer to solid substrates.

In the upstroke the maximum transfer rate of poly(silane) 17 is lower than in the downstroke. This may be the result of the water of the subphase having to flow out of the region between the hydrophobic substrate and the transferred monolayer. As depicted in Figure 11, multilayers are built up in which the polymer backbones are aligned with regard to the dipping direction despite the fact that there is no detectable orientation of the polymer backbones in the monolayer at the water surface. The alignment of the backbones is a result of the transfer process itself, and we assume that the orientation occurs in the region of the meniscus. The molecular orientation of the poly(silanes) in the LB multilayers is represented by the model depicted in Figure 11. The dimensions of the rodlike polymers normal to the plane of the substrate, calculated from this model, agree well with the layer spacing obtained from Bragg reflection. Multiplying the layer spacing with the number of layers gives the same

total thickness of the LB multilayer as obtained from X-ray reflection. This proves the existence of single layers and excludes the formation of double layers as known from poly(glutamate)s.[14] The alignment of the polymer backbones approximately parallel to the dipping direction of the substrate is confirmed by the dichroism of poly(silane) backbone absorption in UV spectroscopy. The orientation of the phenyl rings as depicted in Figure 11a is confirmed by polarized UV and IR spectroscopy. The latter also shows the conformational disorder of the alkyl and alkoxy side chains. This model is consistent with a molecular geometry in which the poly(diphenylsilane)s adopt an all-trans planar zigzag conformation as discussed above.

The improvement in the orientation of the polymer backbones of the LB multilayers that results from annealation must be related to their form anisotropy. This effect is observed in all multilayers with one exception, the very first layer that is adjacent to the substrate. It has a lower dichroic ratio that is not improved by annealing. From the fact that improvements in the orientation are only obtained in multilayers and the fact that the low order of the first layer influences the adjacent layers during annealing, we conclude that interaction between the layers influences the change in orientation of the backbones. This conclusion is supported by the reduction of the layer spacing that occurs during the process of annealing.

Acknowledgment. C. G. Willson thanks the Alexander von Humboldt-Stiftung for providing support in the form of an award. Further help in the synthesis of the polymers by G. Fickes and D. Thompson and helpful discussion with T. Sauer are gratefully acknowledged. Financial support in the framework of the UDS project of the BMFT is acknowledged.

References and Notes

(1) Miller, R. D.; Michl, J. *Chem. Rev.* **1989**, *89*, 1359.
(2) West, R. J. *Organomet. Chem.* **1986**, *300*, 327 and references cited therein.
(3) Miller, R. D.; Hofer, D.; McKean, D. R.; Willson, C. G.; West, R.; Trefonas, P. T. *ACS Symp. Ser.* **1984**, *266*, 293.
(4) Kajzar, F.; Messier, J.; Rosillio, C. *J. Appl. Phys.* **1986**, *60*, 3040.
(5) Baumert, J. C.; Bjorklund, G. C.; Jundt, D. H.; Jurich, M. C.; Looser, H.; Miller, R. D.; Rabolt, J.; Sooriyakumaran, R.; Swalen, J. D.; Twieg, R. J. *Appl. Phys. Lett.* **1988**, *53*, 1147.
(6) Yang, L.; Wang, Q. Z.; Ho, P. P.; Dorsinville, R.; Alfano, R. R. *Appl. Phys. Lett.* **1988**, *53*, 1245.
(7) Sugi, M. *J. Mol. Electron.* **1985**, *1*, 3 and references cited therein.
(8) Embs, F. W.; Funhoff, D.; Laschewsky, A.; Licht, U.; Ohst, H.; Prass, W.; Ringsdorf, H.; Wegner, G.; Wehrmann, R. *Adv. Mat.* **1991**, *3* (1), Special Issue: Organic Thin Films).
(9) Duda, G.; Schouten, A. J.; Arndt, T.; Lieser, G.; Schmidt, G. F.; Bubeck, C.; Wegner, G. *Thin Solid Films* **1988**, *159*, 221.
(10) Duda, G.; Wegner, G. *Makromol. Chem. Rapid Commun.* **1988**, *9*, 495.
(11) Orthmann, E.; Wegner, G. *Angew. Chem.* **1986**, *98*, 114.
(12) Cotts, P. M.; Miller, R. D.; Trefonas, P.; West, R.; Fickes, G. N. *Macromolecules* **1987**, *20*, 1047.
(13) Cotts, P. M.; Miller, R. D.; Sooriyakumaran, R. *Bull. Am. Phys. Soc.* **1988**, *33* (3), 656.
(14) Miller, R. D.; Sooriyakumaran, R. *Macromolecules* **1988**, *21*, 3120.
(15) Foster, M.; Stamm, M. N.; Reiter, G.; Hüttenbach, S. *Vacuum* **1990**, *41*, 1441.
(16) Albouy, P. A.; Sauer, T.; Wegner, G. unpublished results.
(17) Yeh, P. Optical Waves in layered media. *Pure Appl. Opt.* **1988**.
(18) Kjaer, K.; Als-Nielsen, J.; Helm, C. A.; Tippmann-Krayer, P.; Möhwald, H. *Thin Solid Films* **1988**, *159*, 17.
(19) Arndt, T.; Wegner, G. In *Optical Techniques to Characterize Polymer Systems*; Bässler, H., Ed.; Elsevier Science: Amsterdam, 1989; p 41.
(20) Neher, D.; Wolf, A.; Bubeck, C.; Wegner, G. *Chem. Phys. Lett* **1989**, *163*, 116.

Registry No. 1 (homopolymer), 97036-66-3; 1 (SRU), 96228-24-9; 2 (homopolymer), 125121-04-2; 2 (SRU), 125121-32-6; 3 (homopolymer), 125121-05-3; 3 (SRU), 120517-00-2; 4 (homopolymer), 97036-67-4; 4 (SRU), 94904-85-5; 5 (homopolymer), 134735-84-5; 5 (SRU), 117652-58-1; 6 (homopolymer), 125121-07-5; 6 (SRU), 125121-33-7; 7 (homopolymer), 125121-05-3; 7 (SRU), 120517-00-2; 8 (homopolymer), 117652-56-9; 8 (SRU), 107999-70-2; 9 (homopolymer), 31324-77-3; 9 (SRU), 76188-55-1; 10 (homopolymer), 134735-86-7; 10 (SRU), 134735-92-5; 11 (homopolymer), 111939-58-3; 11 (SRU), 107999-72-4; 12 (homopolymer), 97464-14-7; 12 (SRU), 96743-40-7; 13 (homopolymer), 134735-88-9; 13 (SRU), 134708-63-7; 14 (homopolymer), 134735-90-3; 14 (SRU), 134735-93-6; 15 (homopolymer), 116102-75-1; 15 (SRU), 116102-83-1; 16a (homopolymer), 116102-71-7; 16a (SRU), 116102-81-9; 17a (homopolymer), 116102-73-9; 17a (SRU), 116102-82-0; 18, 99635-07-1; 19, 99635-08-2; 20, 134735-91-4.